Observation of Deep Convective Cloud-Top Height and Vertical Temperature Structure of Hurricane Using Hyperspectral Infrared Sounder and its Single-Field-View Retrieval Products

Xiaozhen Xiong*[a], Xu Liu[a], Wan Wu[a]
Liqiao Lei[a,b],Qiguang Yang[a,b], Daniel K. Zhou[a], and Allen M. Larar[a]

[a]NASA Langley Research Center, Hampton, Virginia, 23681, USA
[b] Science Systems and Applications, Inc., Hampton, Virginia 23666, USA

ABSTRACT

A new method utilizing hyperspectral infrared sounders is developed to estimate cloud top height (CTH) for deep convective clouds from hurricane, or tropical cyclone (TC). By analyzing measurements from the Cross-track Infrared Sounder (CrIS), and further validating with radiative transfer simulations, we identified an inverted-V spectral feature in the ozone (O3) band near 9.6 μm, which correlates with deep convective clouds. The depth of this feature can be used to estimate the CTH of a TC's eyewall and surrounding rain bands. This approach effectively captures the cloud structure of the TC. Additionally, a new single Field of View sounder products (SiFSAP), derived from CrIS and the Advanced Technology Microwave Sounder (ATMS), will be used to analyze the vertical temperature and water vapor structure, offering more insights into TC dynamics.

Keywords: Hurricane, deep convective cloud, cloud top height, CrIS, Single-field-view retrieval

1. INTRODUCTION

Clouds play a vital role in the weather and climate system, particularly deep convective clouds, which significantly impact the tropospheric energy cycle, Earth's radiation budget, the transport of water vapor and trace gases into the stratosphere, and precipitation patterns (e.g., Sherwood and Dessler 2001). These effects are highly sensitive to cloud-top height (CTH). Hurricanes, tropical cyclones (TC), or typhoons are major natural disasters, and numerous studies have shown that TC intensity changes are closely linked to deep convective clouds, with stronger TCs associated with higher cloud top heights []. Accurate determination of CTH is crucial for monitoring TC development and understanding TC dynamics.

Various tools are used to measure cloud-top heights, including satellites, LIDAR, and weather balloons. Satellites, in particular passive sensors, provide global observations of cloud properties with high temporal resolution, making them a crucial tool for monitoring clouds in weather and climate research. Satellite-derived CTH data can also be used to evaluate weather and climate models. By analyzing cloud height variations over time and across regions, scientists can improve climate models, predict weather more accurately, and assess the impact of climate change on cloud behavior.

Numerous have been developed to estimate cloud-top height (CTH) using satellite data. These methods include the split-window technique (e.g., Hamada and Nishi, 2010), the tri-window technique (e.g., Heidinger et al., 2010, 2019), the CO_2 slicing method combined with optimal estimation, and more recently, AI-based approaches (e.g., Dong et al., 2022). For optically thick and low clouds, many researchers use radiance fitting with the infrared window channel at 10.8 μm. For semi-transparent or broken clouds it is necessary to employ the radiance ratioing method (Hamann et al., 2014).

For an opaque cloud, one can locate the approximate top by using the satellite measured brightness temperature at atmospheric window region (e.g., 10–12 mm) to match a local atmospheric sounding temperature profile [Smith and Platt, 1978]. Even though this thermally estimated cloud tops are typically 1–2 km lower than lidar data even for optically thicker clouds (Sherwood et al., 2004b), this method is especially useful for optically thick clouds when they are in thermal equilibrium with the surrounding environments, where the thermal emission mainly originates from the uppermost cloud layer [Gupta et al., 2022]. In this paper, we refer to this approach as the "temperature method".

In this study, we aim to develop a new method to estimate CTH using hyperspectral infrared sounders for hurricane or tropical cyclone analysis. Satellite observations from the Cross-track Infrared Sounder (CrIS) on SNPP, J-1, and J-2 will be used. We will utilize collocated ECMWF Reanalysis version-5 (ERA5) data with CrIS measurements to derive CTH for each CrIS pixel, and these CTHs data will be used as a "truth" for this study.

*Xiaozhen.Xiong@nasa.gov; phone 1 410 412-4301; NASA Langley Research Center

2. DATA AND METHOD

CrIS is an advanced Fourier transform spectrometer that measures the thermal infrared radiances in three spectral bands, i.e., the long-wave IR band 1 (648.75–1096.25 cm^{-1}), the mid-wave IR band 2 (1208.75– 1751.25 cm^{-1}), and the short-wave IR band 3 (2153.75– 2551.25 cm^{-1}) (Han et al., 2013, 2015; Goldberg and Zhou, 2017). Since December 14, 2014, CrIS on S-NPP was switched to full spectral mode, which has a spectral resolution of 0.625 cm^{-1} in all three bands and 2211 channels in total. CrIS on J-1 was launched on November 18, 2017. The nadir footprint of CrIS is ~15 km, and each CrIS on S-NPP or J-1 provides near global coverage twice daily. To remove the ringing effects, as is done for the assimilation of CrIS data into Numerical Weather Prediction (NWP) models, a hamming apodization is applied to the CrIS data used in this paper [Han et al., 2015; Borg et al., 2023].

A new single Field of View sounder products (SiFSAP) are derived from CrIS and the Advanced Technology Microwave Sounder (ATMS) for each CrIS pixel with a spatial resolution of ~15 km at nadir (Wu et al., 2023). Traditionally, a few algorithms have been developed to generate atmospheric temperature, water vapor, O_3 and other trace gas products with a coarser spatial resolution than SiFSAP. These algorithms include the *NOAA Unique Combined Atmospheric Processing System* (*NUCAPS*) (e.g., Nalli et al., 2018) and the Community Long-Term Infrared Microwave Combined Atmospheric Product System (CLIMPCAPS) (Smith and Barnet, 2019; 2020). Both have some heritage from the original AIRS algorithm (Susskind et al., 2003, 2014; Xiong et al., 2008, 2014) that relies on the cloud clearing (CC) method to convert 9 field-of-view (FOV) radiance spectra within one Field-of-Regard (FOR) into a cloud-cleared radiance spectrum, resulting in a spatial resolution of approximately 45 km at nadir. Different from the above two approaches, SiFSAP products are derived in each FOV without using the CC method (Zhou et al., 2005; 2007). The SFOV retrieval algorithm is based on PCRTM and an optimal estimation retrieval method (Liu et al., 2006, 2007, 2009, 2016; Wan et al., 2017, 2019; 2022). As PCRTM includes accurate computation of cloud multiple scattering, which uses cloud lookup tables calculated by 32-stream DIScrete Ordinates Radiative Transfer (DISORT) model (Stamnes et al., 1988), this algorithm retrieves cloud properties (phase, optical depth, droplet size and cloud height) together with atmospheric temperature and water vapor profiles simultaneously. Another difference is that NUCAPS and CLIMCAPS use only a portion of the channels selected from the 2211 CrIS channels, whereas the SiFSAP algorithm uses information from all spectral channels by compressing all channel radiances into the PC domain. In general, the information content of a CrIS spectrum can be captured by the first 120-160 PCs, and the retrievals are made in PC-domain space using these PCs, which helps to reduce the apparent noise of the retrieval products and speed up the inversion process. The combined use of microwave sensor, i.e. ATMS, and CrIS allows for accurate retrievals under cloudy conditions. More detail about SiFSAP can be obtained from Wu et al. (2023). Some advantages of using SiFSAP products for process-oriented analysis of the weather events, such as stratospheric intrusion and cold air outbreak, have been previously demonstrated by Xiong et al. (2022a, -b).

Two reanalysis products are also used for analysis. The first is the NASA Modern-Era Retrospective Analysis for Research and Applications, Version 2 (MERRA-2), which has a spatial resolution of 0.5°X0.625° latitude-by-longitude grid with a 3-hour interval and 72 model layers up to 0.01 hPa. Another is ERA-5, which has a resolution of 0.25°X0.25° latitude-by-longitude grid with a 1-hour interval. To match the reanalysis data with CrIS measurements, differences between the models and CrIS in both temporal and spatial domains were accounted for. For temporal difference, a linear interpolation was first made between the 3-hour interval of the MERRA-2 reanalysis data and the 1-hour interval between the ERA-5 reanalysis data bounding the pixel of CrIS observation. Then, the data were interpolated to the center of each FOV of CrIS to match with CrIS observation. Using ERA-5 temperature profile collocated with CrIS and the brightness temperature at 11 μm (BT11) measured by CrIS, we can estimate the cloud top height by linearly interpolating BT11 to ERA-5 temperature profile.

Aumann et al. (2011) discovered that for some extremely cold cloud tops, where BT1231 (8.1 μm) is below 210 K, the observed spectra were inverted compared to clear sky cases. To better understand the impact of clouds on the spectra, we used the PCRTM model to simulate the CrIS spectra. In addition to cloud properties, the inputs to the model also include temperature, water vapor and ozone profiles from the ERA-5 matched with the CrIS observation. Figure 1 shows an example of the temperature profile used, and the cloud tops are marked using different horizonal lines. For cloud top at 540 hPa, it is assumed to be a water cloud with an effective diameter (De) of 12 micron, and all other clouds with tops at higher altitudes are assumed as one-layer ice cloud with a De of 30 μm. All cloud optical depths are set as 6, which is thick enough based on our SiFSAP retrieved cloud properties, and the surface emissivity is assumed to be 0.97. It is evident from Figure 1 that, as expected, the spectra for low water clouds are similar to clear sky (dark dash line), and they both have a deep "V" feature near 9.6 μm. With the cloud tops moving up to higher altitude of about 200-250 hPa, the spectra become inverted and the inverted "V" become deeper until the cloud top moves closer to tropopause. The peak height of the inverted "V" is relatively small for the cloud with top at 215 hPa, and it increases with cloud top increases. Here we introduce a new variable called "height index" (H_index), which is defined as the difference between the maximum BT within the spectra range of 995-1065 cm^{-1} (or 10.1 - 9.4 μm) and the minimum of BT within the same spectral range. The maximum BT occurs at 1050.625 cm^{-1} (9.52 μm) and is designated as BT1051, while the minimum BT is located near the center of this spectral range at 1042.5 cm^{-1}(9.59 μm), which is the most transparent channel in the ozone band near 9.6 μm. For non-inverted spectra over low water clouds or clear skies, H_index of less than 0, and H_index reaches its maximum when the cloud top is near the tropopause.

Figure 2 displays the H_index map for Hurricane Ian at approximately 07 UTC on September 28, 2022, along with the spectra associated with different H_index values. The spectra show an inverted shape for H_index values of 5, 10, and 15, compared to an H_index of -5. It is also apparent that the heights of the inverted spectra near 9.6 μm increase as H_index rises from 5 to 10 and then to 15. Figure 3 illustrates the cloud-top height (CTH) derived using collocated ERA-5 temperature profiles, and the right panel of Figure 3 demonstrates a strong correlation between H_index and CTH. In Figure 3, we also include CTH calculated using SiFSAP-retrieved temperature (from ATMS) data for Hurricane Ian. As shown, H_index values are primarily less than 0 for clouds with CTH below 10 km and increase nearly linearly as CTH rises, achieving a correlation of 0.96. H_index reaches approximately 15 for cloud tops near the tropopause. This strong correlation between H_index and CTH suggests that H_index can effectively estimate CTH for deep convective clouds in hurricanes. Based on a linear fit of CTH with various parameters, we derive the following empirical relation:

$$CTH = c0 + c1 * H_{index} + C2 * BT11 + C3 * Sin(VZA) + C4 * BTD$$

Where BT11 is the brightness temperature measured by CrIS with a unit (°C), VZA is satellite viewing angle, and $BTD=BT_{961}-BT_{790}$. For this case using the CrIS descending data for hurricane, (c0,c1,c2,c3,c4) = (7.079, 0.080, -0.082,-0.521, 0.070).

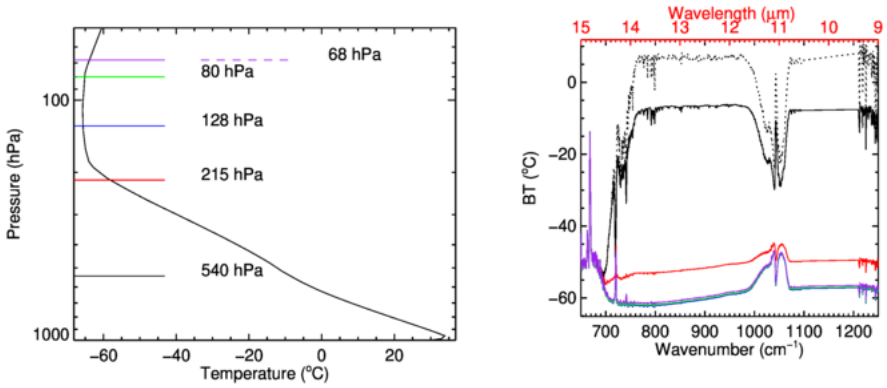

Figure 1. Temperature profile from ERA5 (left) and the PCRTM-simulated spectra (right). Different colors for the spectra correspond to clouds with different top heights with the same color lines in the left panel. Dash dark line in the right is for clear sky, and pink dash line is for ice cloud with De=30 μm.

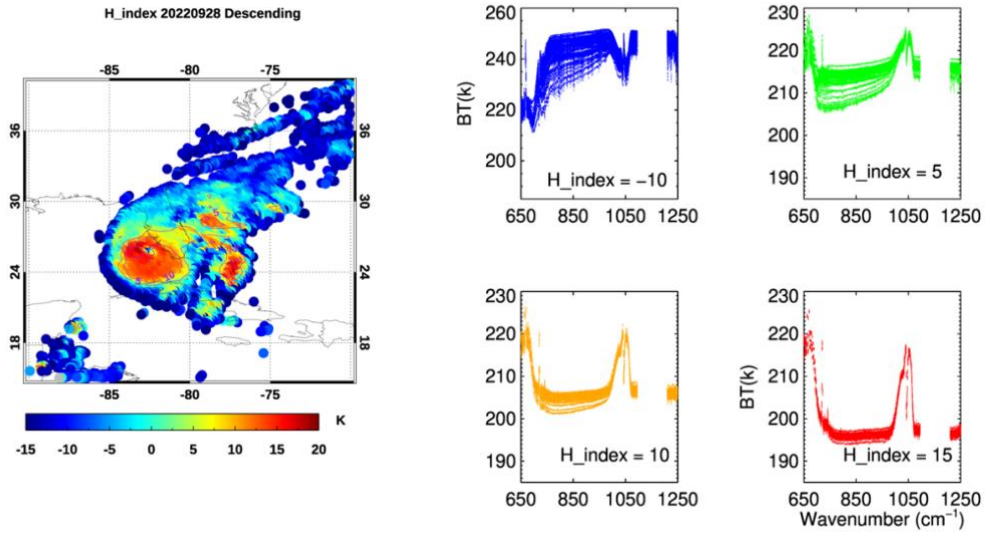

Figure 2. Map of H_index and the CrIS-measured spectra corresponding to different H-index. The colors of the spectra in the right panels are close to the colors of H_index in the map. Data used is from the descending of hurricane Ian.

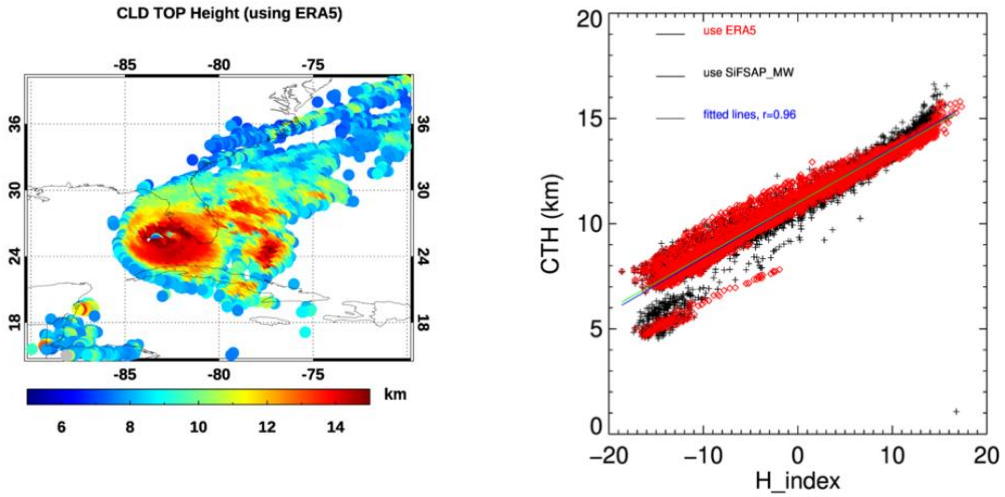

Figure 3. . Map of CTH derived from BT11 from CrIS (left) and the correlation between H_index (shown in Figure 2) and CTH estimated using ERA-5 temperature profiles and SiFSAP microwave retrieved temperature profiles. Data used is from the descending of Cris for hurricane Ian.

3. RESULTS AND DISCUSSION

Using data from the descending pass of CrIS on J-1 for Hurricane Ian, we derived cloud-top height (CTH) by fitting CrIS BT11 values to collocated ERA-5 temperature profiles. A linear fit was performed using data with H_index > 0 to obtain the coefficients, which were then applied to all CrIS data with BT11 < -20°C that represent clouds of sufficient thickness. The CTH map produced by this new method closely matches the temperature method derived CTH (shown in Figure 3), with their differences displayed in the middle of Figure 4, along with a scatter plot of absolute and relative differences versus H_index on the right panel. The error in CTH from this new method is mostly within 1 km or 5%, with a mean error of -0.017 ± 0.186 km (or -0.19 ± 2.04%). A larger error occurs for H_index < -10, corresponding to thinner low-level water clouds.

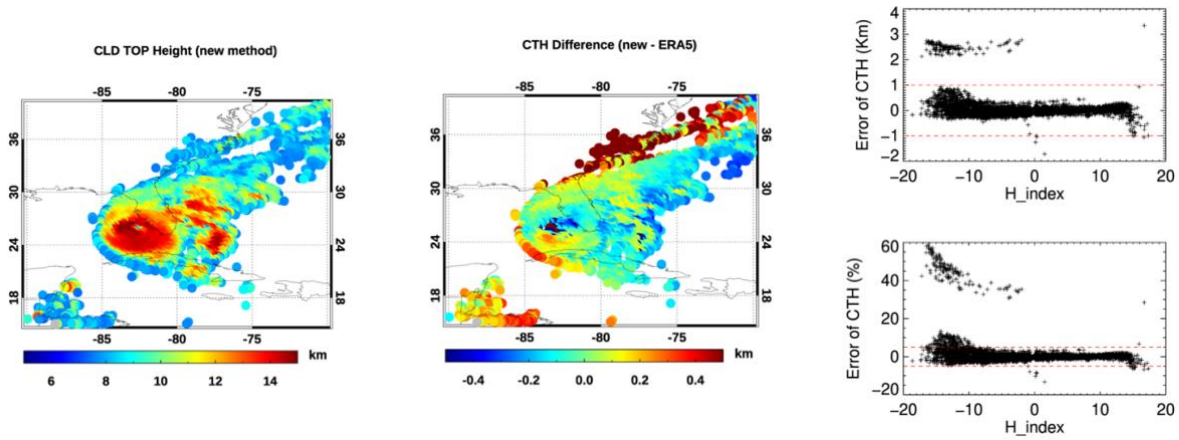

Figure 4. Map of CTH derived from using the new method (Eq. (1) and its difference from that using ERA-5 temperature profiles. Right panel is the scatter plot of absolute and relative CTH difference between these two methods with H_index. Data used is from the descending of hurricane Ian.

To validate, we applied the coefficients derived from the CrIS descending observation to the CrIS ascending observation approximately 12 hours later for Hurricane Ian. The resulting errors, shown in Figure 5, are similar to those for the descending

data. Near the eyewall, the estimated CTH is 0.2–0.3 km lower than the temperature method, with a mean error of -0.361 ± 0.167 km (or -0.24 ± 1.77%), demonstrating the robustness of this method.

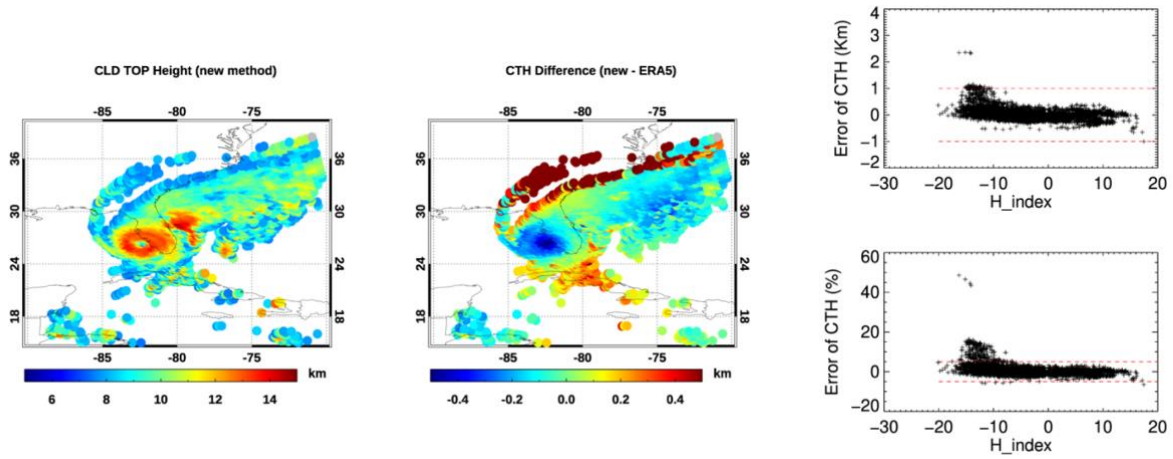

Figure 5. Same as Figure 4 but using the data of the CrIS of ascending for hurricane Ian.

We further applied this method to the recent Hurricane Helene, the strongest hurricane on record to strike Florida's Big Bend region and the deadliest to impact the mainland U.S. since Katrina in 2005. Hurricane Helene began forming on September 22 as a broad low-pressure system in the western Caribbean Sea. It developed into a hurricane early on September 25, 2024, and reached Category 4 intensity on the evening of September 26 before weakening as it quickly moved inland, eventually degenerating into a tropical cyclone over Tennessee on September 27. Figure 6 shows the CTH of Helene over three days. The presence of high clouds over the rain bands is evident on September 25, and the thick clouds near the eyewall are evident on September 26. Comparison of CTH values shows that CTH increases as the hurricane intensifies from September 25 to 26 and decreases as it weakens at September 27.

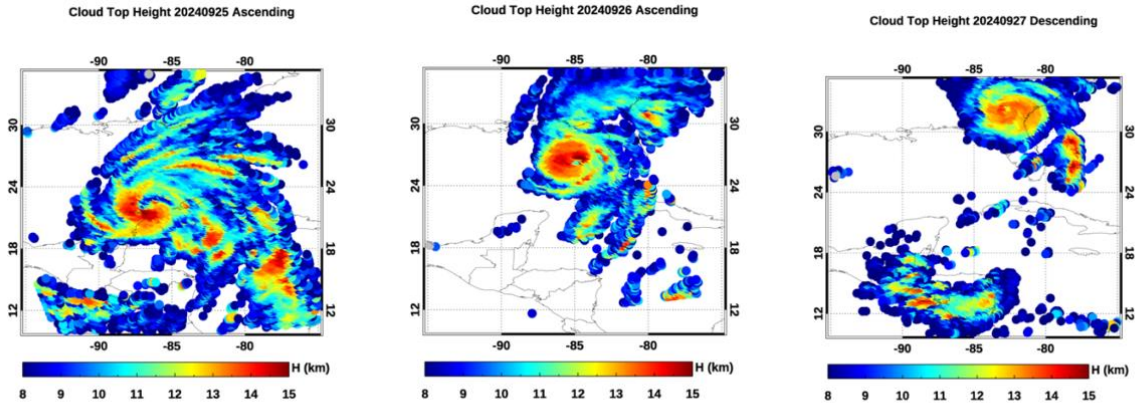

Figure 6. Images of CTH estimated using eq.(1) for hurricanes Helene . Only one image is shown as example for each hurricane.

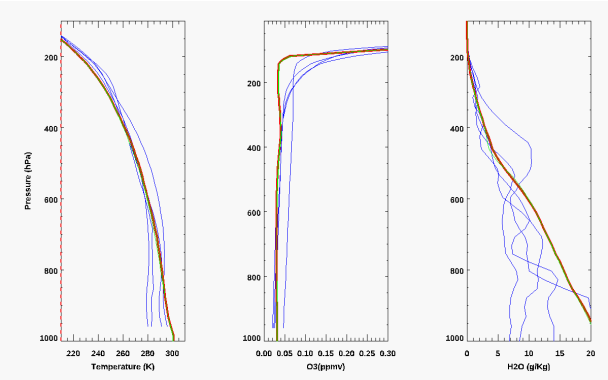

Figure 7. SiFSAP retrieved temperature, ozone and water vapor profiles near the eye of hurricane Ian (blue lines) using CrIS ascending data on 18:30 UTC. For comparison the collocated profiles of temperature, ozone and water vapors from MERRA-2 and ERA-5 are plotted using red and green lines, respectively.

Due to the typically thick clouds in hurricanes, retrieving temperature and water vapor profiles using infrared sensors is highly challenging. However, the Single Field of View Sounder Atmospheric Products (SiFSAP), with a smaller spatial resolution of approximately 14 km, allows for retrievals closer to the hurricane eye than other operational sounder products. Figure 7 shows the SiFSAP-retrieved temperature, ozone, and water vapor profiles, along with comparisons to collocated MERRA-2 profiles. Overall, the retrieved temperature profiles agree reasonably well with MERRA-2, though SiFSAP shows significant variability in water vapor, highlighting the challenges of H_2O retrieval. The retrieved ozone near 200 hPa is lower than model simulations, consistent with findings that deep convection in hurricanes can transport lower-ozone tropospheric air to the lower stratosphere. We also used SiFSAP microwave-retrieved temperature profiles and BT11 fitting to estimate retrieved CTH for CrIS descending and ascending observations. The mean differences between CTH calculated using eq. (1) and retrieved CTH are 0.079 ± 0.423 km (1.01 ± 3.51%) for descending and 0.094 ± 0.327 km (1.17 ± 3.46%) for ascending observations.

4. SUMMARY AND CONCLUSIONS

We developed a new method using hyperspectral infrared spectra to estimate the cloud-top height (CTH) of hurricanes. By analyzing infrared spectra measured by the Cross-track Infrared Sounder (CrIS) for Hurricane Ian, we identified an inverted-V spectral feature in the ozone (O_3) band near 9.6 μm that correlates with deep convective clouds, and this inverted spectrum feature was further validated using radiative transfer simulations. Using CrIS data from Hurricane Ian, it is found that the correlation coefficient of the depth of this invert V feature with CTH, i.e. H_index, is over 0.96. Using CTH obtained by traditional temperature method that fitting the brightness temperature from thermal infrared channels in the atmospheric window to collocated ERA-5 temperatures, we derived an empirical equation to compute CTH using H_index and three additional variables. The error in CTH from this new method is mostly within 1 km or 5%, with a mean error of -0.017 ± 0.186 km (or -0.19 ± 2.04%). Higher errors are observed for H_index < -10, which corresponds to thinner, lower water clouds.

Applying this method to estimate the CTH of Hurricane Helene demonstrated its effectiveness in capturing the cloud structure of hurricanes. Additionally, we used a new single Field of View Sounder Atmospheric Product (SiFSAP) derived from CrIS and ATMS. Comparison of retrieved temperature, water vapor, and ozone profiles near the hurricane eye with ERA-5 and MERRA-2 data showed reasonable agreement in temperature retrievals, though water vapor retrieval remains challenging.

This study provides a simple, effective method for estimating hurricane CTH using hyperspectral sounders, which can be applied for operational monitoring of hurricane cloud structures. The single-field-of-view sounder product using hyperspectral infrared and microwave data offers further insights into the temperature structure of tropical cyclones.

ACKNOWLEDGEMENTS

This research was partially supported by the NASA NAST-I program, and the authors wish to acknowledge Dr. J. A. Kaye of the NASA *Science Mission Directorate* for his continued enabling support. Resources supporting this work were provided by the NASA High-End Computing (HEC) Program through the NASA Advanced Supercomputing (NAS) Division at NASA Ames Research Center.

REFERENCES

[1] Hamann, U. Remote sensing of cloud top pressure/height from SEVIRI: analysis of ten current retrieval algorithms. Atmos. Measurement Techniques, 7(9), 2839-2867 (2014).
[2] Sherwood, S. C., Chae, J.-H., Minnis, P., and McGill, M.: Underestimation of deep convective cloud tops by thermal imagery, Geophys. Res. Lett., 31, L11102, doi:10.1029/2004GL019699, 2004.
[3] Sherwood, S. C., P. Minnis, and M. McGill (2004), Deep convective cloud-top heights and their thermodynamic controlduring CRYSTAL-FACE, J. Geophys. Res., 109, D20119, doi:10.1029/2004JD004811
[4] Smith, W. L., and C. M. R. Platt, 1978: Comparison of satellite deduced cloud heights with indications from radiosonde and ground-based laser measurements. J. Appl. Meteor., 17, 1796–1802.
Hamada, A.; Nishi, N. Development of a Cloud-Top Height Estimation Method by Geostationary Satellite Split-Window Measurements Trained with CloudSat Data. *J. Appl. Meteorol. Clim.* **2010**, *49*, 2035–2049.
[5] Christopher D. Barnet. et al., "The NOAA Unique CrIS/ATMS Processing System (NUCAPS): Algorithm Theoretical Basis Documentation," https://star.nesdis.noaa.gov/jpss/documents/AT BD/ATBD_NUCAPS_v3.1.pdf, 2021
[6] Smith, N., Barnet, C.D., "Uncertainty Characterization and Propagation in the Community Long-Term Infrared Microwave Combined Atmospheric Product System (CLIMCAPS)," *Remote Sens*., vol. 11, pp. 1227, 2019
[7] Wu, W, X. Liu, X. Xiong, Q. Yang, A. Lara, D. K. Zhou, 2022: Single Field-of-view Sounding Atmospheric Products. *2022 IEEE International Geoscience and Remote Sensing Symposium (IGARSS)*.
[8] Gupta, A. K., Bennartz, R., Fauria, K. E., and Mittal, T. (2022). Timelines of plume characteristics of the Hunga Tonga-Hunga Ha'apai eruption sequence from 19 December 2021 to 16 January 2022: Himawari-8 observations. Earth Space Sci. Open 'rchive. doi:10.1002/essoar.10510853.2.
[9] M. Goldberg and L. Zhou, "The joint polar satellite system — Overview, instruments, proving ground and risk reduction activities," *2017 IEEE International Geoscience and Remote Sensing Symposium (IGARSS)*, Fort Worth, TX, 2017, pp. 2776-2778, doi: 10.1109/IGARSS.2017.8127573.
[10]Liu, X., W. L. Smith, D. K. Zhou, and A. Larar, "Principal component-based radiative transfer model for hyperspectral sensors: theoretical concept," *Appl. Opt.* 45, 201-209, 2006.
[11]Wu, W., Liu, X., Lei, L., Xiong, X., Yang, Q., Yue, Q., Zhou, D. K., and Larar, A. M.: Single field-of-view sounder atmospheric product retrieval algorithm: establishing radiometric consistency for hyper-spectral sounder retrievals, Atmos. Meas. Tech., 16, 4807–4832, https://doi.org/10.5194/amt-16-4807-2023, 2023